Structural basis for high-pressure polymorphism in $CuGeO_3$

Przemyslaw Dera, Aiyasami Jayaraman, Charles T. Prewitt, and Stephen A. Gramsch
Geophysical Laboratory and Center for High Pressure Research, Carnegie Institution of Washington, 5251 Broad Branch Road, NW, Washington, D.C. 20015

(Received 5 July 2001; revised manuscript received 5 December 2001; published 19 March 2002)

Two unusual pressure-induced structural transformations in the inorganic spin-Peierls compound $CuGeO_3$ have been studied using single-crystal x-ray diffraction and diamond-anvil cell techniques. $CuGeO_3$-III was formed after nonhydrostatic compression of the ambient pressure phase $CuGeO_3$-I and the structure determined after quenching back to ambient pressure from 7.0 GPa. $CuGeO_3$-III is orthorhombic, with space group $Pbam$. The mechanism of the I-III transformation, which occurs exclusively under nonhydrostatic conditions, involves a shift of half of the Ge atoms to tetrahedral sites adjacent to those occupied in the ambient pressure modification. Hydrostatic compression of $CuGeO_3$-III from ambient conditions to near 7.0 GPa results in the formation of monoclinic $CuGeO_3$-IV, with space group $P2_1/c$. Upon compression, the Ge atoms in $CuGeO_3$-IV adopt an approximately trigonal bipyramidal coordination environment, formed by the condensation of two tetrahedral sites. Our findings provide a basis for the formulation of a general mechanism explaining the pressure-induced transformations in $CuGeO_3$ and their sensitivity to deviatoric stress.

DOI: 10.1103/PhysRevB.65.134105 PACS number(s): 81.40.Vw, 61.50.Ks

I. INTRODUCTION

Copper metagermanate ($CuGeO_3$) has attracted a great deal of attention in recent years, particularly because it is the first known example of an inorganic system exhibiting a spin-Peierls transition at low temperature.[1] The crystal structure of the ambient pressure and temperature phase, $CuGeO_3$-I, presented in Fig. 1, is orthorhombic (*Pbmm*) with unit cell $a=4.8022(6)$ Å, $b=8.4739(7)$ Å, $c=2.9433(3)$ Å.[2–4] An electron paramagnetic resonance (EPR) study[5] revealed the existence of a spin pairing (antisymmetric exchange) interaction between Cu^{2+} moments, which is forbidden in centric space groups. Re-examination of the structure of $CuGeO_3$-I with carefully annealed crystals revealed superlattice reflections, and a different, acentric structure model was proposed, with space group $P2_12_12_1$, and an eightfold increase in unit-cell volume ($a_a=2a_c$, $b_a=b_c$, $c_a=4c_c$).[6] That proposal, however, has later been questioned, because no sign of a superlattice has been found in further neutron diffraction experiments.[3] As a result of the interest in characterizing structural and physical properties relevant to the spin-Peierls phenomenon, the structure of $CuGeO_3$ has also been studied at different thermodynamic conditions.[7–9] Pressure was found to influence the spin-Peierls effect quite strongly.[10–13] A high-pressure–low-temperature phase $CuGeO_3$-Ib (no spin-Peierls effect, $T<180$ K, $3<P<6$ GPa) was observed by Raman spectroscopy.[14] Other experiments[15] have not confirmed the existence of $CuGeO_3$-Ib, but revealed two other interesting high-pressure–low-temperature phases, $CuGeO_3$-III$_{sp}$ and $CuGeO_3$-III, at pressures of 1.6-6.0 GPa, both of which transform to another phase, $CuGeO_3$-II, at pressures greater than 6 GPa. Ambient-temperature–high-pressure experiments revealed that structural changes taking place in $CuGeO_3$ are strongly dependent on the hydrostaticity of the pressure medium. Raman spectroscopy[14,16–18] indicates that during quasihydrostatic compression $CuGeO_3$-I transforms to $CuGeO_3$-III,[19] near 7 GPa, and $CuGeO_3$-IV, at about 8 GPa, while during hydrostatic compression there is only one phase transformation in this pressure region, to $CuGeO_3$-II.

A high-pressure x-ray diffraction study on $CuGeO_3$ was carried out using the energy-dispersive synchrotron powder diffraction (EDX) method.[21] These authors observed the I-II phase transition near 7 GPa, and indexed the diffraction data for the high-pressure phase on the basis of a monoclinic unit cell, with space group $P2_1/a$. Later, hydrostatic compression of phase I was studied using the angular-dispersive synchrotron powder diffraction (ADX),[22] and revealed the compression behavior of phase I, but left the structure of phase II

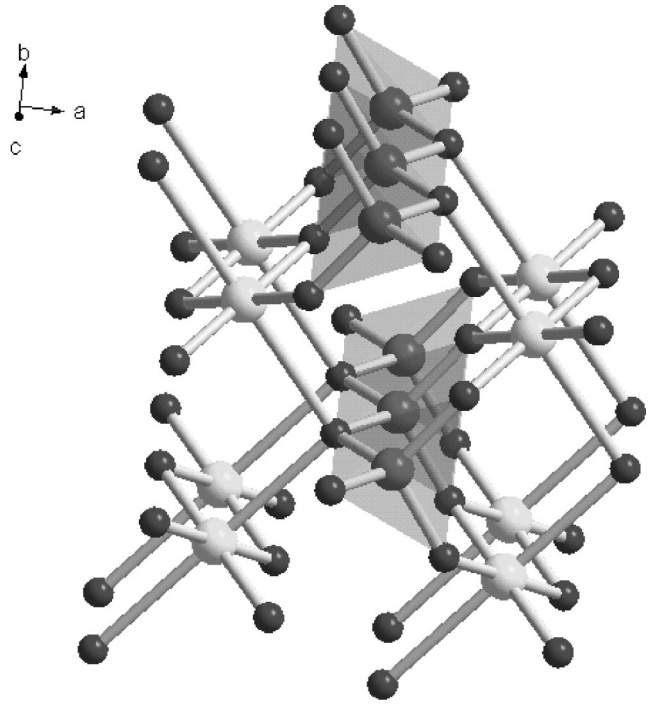

FIG. 1. The crystal structure of $CuGeO_3$-I viewed along **c**.

unsolved. Neutron-diffraction experiments[23] confirmed the compression behavior of $CuGeO_3$-I up to 6.2 GPa. Recently, based on synchrotron EDX studies of $CuGeO_3$ powder, unit cells for phases II, III, and IV, and for some higher-pressure phases, were proposed.[24] Most recently, results of a single-crystal XRD study under hydrostatic conditions were reported[4] and a model for the crystal structure of phase II at 6.5 GPa proposed. Because of the problems with retaining the single-crystal character of nonhydrostatically compressed specimens, the structures of $CuGeO_3$-III and $CuGeO_3$-IV have not been determined, despite the fact that $CuGeO_3$-III is quenchable. $CuGeO_3$-II and $CuGeO_3$-III have completely different Raman spectra, yet form at essentially the same pressure, suggesting a metastability associated with the phase transformation of $CuGeO_3$-I induced by nonhydrostatic compression, as well as the presence of other, perhaps equally accessible phases in the $CuGeO_3$ system. The crystal chemistry of these two phases is therefore of considerable interest, as is the behavior of quenched $CuGeO_3$-III under hydrostatic compression. The main objective of the present work was, through a very careful application of pressure and using a suitable quasihydrostatic pressure medium, to isolate and quench a single crystal of $CuGeO_3$-III, and solve the crystal structure. In addition, a secondary goal was to investigate the high-pressure behavior of $CuGeO_3$-III under hydrostatic compression and to understand the crystal chemistry of the phases present in this system.

II. EXPERIMENT

A. Synthesis of $CuGeO_3$-I and $CuGeO_3$-III

Clusters of $CuGeO_3$ crystals containing an assortment of sizes were made available to us by Dr. S.-W. Cheong of Lucent Technologies, Bell Laboratories. Single crystals of $CuGeO_3$ were grown using a stoichiometric mixture of CuO and GeO_2. At 1150 °C $CuGeO_3$ melts congruently; the melt was cooled slowly in the range 1150–1130 °C and then more quickly from 1130° to room temperature. The resulting crystals of $CuGeO_3$-I were of a plateletlike habit, pale blue in color and very soft. Three suitable single crystals of phase I were chosen on the basis of optical examination and tests of the quality of their diffraction patterns. Each crystal was loaded into a Mao-Bell-type diamond-anvil cell containing diamonds with 800-μm culets and a stainless steel gasket with a hole 300 μm in diameter. To produce quasihydrostatic conditions in the sample chamber, glycerin was used as the pressure-transmitting medium. The sample was then pressurized carefully until it changed color from pale blue to deep blue, indicating the transition from phase I to phase III. Pressure was then very slowly released to preserve the single crystal.

B. Compression of $CuGeO_3$-III

A Merrill-Bassett-type diamond-anvil cell was used in the experiments, equipped with 800-μm-culet diamonds fixed to beryllium metal seats and a stainless-steel gasket with a 300-μm-diameter hole for the sample. A single crystal of quenched $CuGeO_3$-III was then loaded into the sample chamber with a 4:1 ethanol-methanol mixture as the hydrostatic pressure-transmitting medium. Three small ruby grains were also included for the purpose of pressure determination by the ruby fluorescence method. The diffraction data were collected at 1.6, 3.2, and 4.5 GPa. At approximately 7.0 GPa the sample abruptly changed color from pale blue to deep blue, indicating the transition from phase III to a new phase ($CuGeO_3$-IV). Diffraction data sets for $CuGeO_3$-IV were collected at 7.4 and 7.6 GPa; when the pressure was increased above 8.0 GPa, the thickness of the stainless-steel gasket became too small to contain the sample, and the single crystal was crushed between the diamond anvils.

C. Data collection

All diffraction experiments were carried out using a Bruker AXS P4 automated diffractometer and a SMART 1 K charge-coupled device (CCD) detector. Mo $K\alpha$ radiation was produced by a graphite monochromator, with a sample-to-detector working distance of approximately 70 mm. Diffraction images were collected in a standard, predefined series of six scans containing a total of 1650 frames (0.3° each) for ambient pressure experiments and a custom series of eight scans (ω scans at $\chi=0$, 30, 60, and 90° with $\phi=0$ and 90°, $2\theta=25°$) containing a total of 2200 frames for high-pressure experiments. For the evaluation of lattice parameters, shorter runs with just two scans ($\chi=0$ and 90°, with $\phi=0°$) were used. Diffraction data were collected for a counting time of 10 s (ambient) or 30 s (high pressure). Data were corrected for geometrical distortion, dark current and flood-field effects. For ambient pressure experiments, the crystal orientation was determined by a routine in the SMART program (Bruker AXS); for diamond-anvil cell experiments, the HP suite of programs (Dera, in preparation) allowed a determination of the sample orientation. An absorption correction was applied with the programs SADABS (Bruker AXS) for ambient pressure data and DACabs (empirical correction, Dera, in preparation) for the diamond-anvil cell data.

D. Structure solution and refinement

Structures of both phases III and IV were solved using direct methods capabilities of the program SHELXS,[25] from the SHELXTL package. Refinements were carried out using the SHELXL program from the same package. Data from three different sample crystals were analyzed independently to determine the structure of $CuGeO_3$-III, giving results consistent within experimental error. Details of structure refinement are given in Table I. After solving the structure in orthorhombic space group $Pbam$ with $a=10.052(2)$ Å, $b=8.192(2)$ Å, and $c=5.795(1)$ Å ($a_{III}=2a_I, b_{III}=b_I, c_{III}=2c_I$), locating the positions of all the atoms resulting from stoichiometry, and refining the model with anisotropic displacement parameters, the reliability factor R_1 was still in the vicinity of 10%. Moreover, two strong peaks with intensities close to 10 eÅ^{-3} remained in the difference Fourier map. The structure model of $CuGeO_3$-III resulting from this refinement involved a change in the geometry of Ge chains compared to $CuGeO_3$-I, with every other Ge tetrahedron

TABLE I. Crystal data and structure refinements for $CuGeO_3$-III and $CuGeO_3$-IV.

Pressure	0.1 MPa	7.6 GPa
Crystal system, space group	orthorhombic, $Pbam$	monoclinic, $P2_1/c$
Unit-cell dimensions	$a=10.052(2)$ Å	$a=4.783(3)$ Å
	$b=8.192(2)$ Å	$b=6.718(4)$ Å
	$c=5.795(1)$ Å	$c=6.157(4)$ Å
		$\beta=92.387(14)°$
Volume	477.21(18) Å^3	197.64(19) Å^3
Z, calculated density	8, 5.126 Mg/m^3	4, 6.188 Mg/m^3
Absorption coefficient	21.219 mm^{-1}	25.617 mm^{-1}
Range	4.05 to 25.01°	6.07 to 23.40°
Limiting indices	$-11<=h<=10$,	$-2<=h<=2$,
	$-9<=k<=9$,	$-6<=k<=6$,
	$-6<=l<=2$	$-6<=l<=6$
Refl. collected/unique	1992 / 447	250 / 55
	$[R_{int}=0.0719]$	$[R_{int}=0.0743]$
Data/restraints/parameters	447/0/70	55/10/20
Goodness-of-fit on F^2	1.036	1.629
Final R indices $[I>2\sigma(I)]$	$R_1=0.0383$,	$R_1=0.0478$,
	$wR_2=0.0906$	$wR_2=0.1309$
R indices (all data)	$R_1=0.0553$,	$R_1=0.0575$,
	$wR_2=0.0965$	$wR_2=0.1320$
Extinction coefficient	0.0022(6)	0.07(2)
Largest diff. peak and hole	1.176 and -0.880 eÅ^{-3}	0.891 and -0.875 eÅ^{-3}

shifted to a tetrahedrally coordinated site unoccupied in phase I. The arbitrary choice of which Ge^{4+} ions stay in place and which shift results in two possible mirror-image-related Ge-layer structures, with very minor differences in oxygen atom positions. This phenomenon may lead to formation of stacking faults, or macrodomains inside the crystal. The positions of the two extra peaks in the difference Fourier map suggested that, indeed, they could belong to Ge^{4+} in layers that are inverse with respect to the ones described by the initial model.[20] The revised structure model, based on the assumption of inverse-layer existence, included two additional partially occupied Ge^{4+} positions [Ge(12) and Ge(22)]. The structure refinement of this model brought the R factor to the vicinity of 5%, with resulting proper-to-inverse layer ratio $P/I=6.6$ (86.7% of proper layers). For the second and third sample of $CuGeO_3$-III, the structure refinements proceeded similarly to the first, each requiring the layer-disorder model, and giving a comparable P/I ratio. It is interesting to note that the $CuGeO_3$-I superstructure[6] was found to contain adjacent GeO_4 tetrahedra in chains tilted with respect to one another, the arrangement repeating every fourth tetrahedron. This observation may be interpreted as a tendency of the chains of GeO_4 tetrahedra to minimize Ge-Ge repulsion by distortion of the ideal symmetry that exists even in phase I at ambient conditions.

The structure of phase IV was also solved using direct methods. $CuGeO_3$-IV belongs to space group $P2_1/c$, with unit-cell parameters $a=4.783(3)$ Å, $b=6.718(4)$ Å, $c=6.157(4)$ Å, and $\beta=92.439(14)°$ at 7.4 GPa ($a_{IV}=1/2a_{III}$, $b_{IV}=b_{III}$, $c_{IV}=c_{III}$). As the number of symmetry-independent reflections with $I/\sigma>2$ was relatively small, refinement was performed with isotropic displacement parameters (IDP's), and included restraints relating IDP's of ions placed close together. Details concerning structure refinement of both $CuGeO_3$-III and $CuGeO_3$-IV are given in Tables I and II. The specific layered structure of $CuGeO_3$ crystals results in a plateletlike crystal habit. This crystal morphology combined with a restricted accessibility to the reciprocal space in a diamond-anvil cell during an *in situ* data collection results in large standard deviation of the fractional atomic coordinates determined from the structure refinement for $CuGeO_3$-IV. In addition to these effects, the layered structure exhibits a tendency to high mosaicity and development of stacking faults. Yoshiasa *et al.*[4] mentioned the difficulties in obtaining any reasonable *in situ* data (it was necessary to use an area detector). They observed similar effects regarding experimental errors to be present in their study of hydrostatic phase II. The standard deviations they present, including much higher values for x fractional coordinates, are analogous to ours.

III. RESULTS AND DISCUSSION

A. The crystal structure of $CuGeO_3$-III and its relationship to $CuGeO_3$-I

The crystal structure of $CuGeO_3$-I consists of one-dimensional chains of distorted CuO_6 octahedra sharing opposite edges in the equatorial plane of the octahedron, with neighboring chains then sharing apical vertices to form rippled layers, as illustrated in Figs. 1 and 2(a). Chains of this type have been found in Li_2CuO_2,[26,30] $La_{14-x}Ca_xCu_{24}O_{41}$,[27] $Sr_{14}Cu_{24}O_{41}$,[28] and $CuSiO_3$.[29,31] In

TABLE II. Fractional atomic coordinates and equivalent isotropic displacement parameters ($Å^2 \times 10^3$) for $CuGeO_3$. $U(eq)$ is defined as one-third of the trace of the orthogonalized U_{ij} tensor. SOF is the site occupation factor.

Atom	x	y	z	$U(eq)$	SOF
		$CuGeO_3$-III at 0.1 MPa			
Ge(11)	0.2082(2)	0.2615(2)	0.0000	9(1)	0.87
Ge(21)	0.2639(2)	0.1534(2)	−0.5000	10(1)	0.87
Ge(12)	0.266(2)	0.154(3)	0.0000	42(8)	0.13
Ge(22)	0.211(2)	0.256(3)	−0.5000	32(7)	0.13
Cu(1)	0.0000	0.0000	0.2501(3)	15(1)	1.00
Cu(2)	0.5000	0.0000	0.2498(3)	14(1)	1.00
O(1)	0.1029(10)	0.0934(12)	0.0000	18(2)	1.00
O(2)	0.3806(9)	−0.0537(13)	0.0000	18(2)	1.00
O(3)	0.3106(7)	0.2619 (7)	−0.2477(10)	14(2)	1.00
O(4)	0.0940(9)	0.1069(11)	−0.5000	13(2)	1.00
O(5)	0.3704(9)	-0.0176(11)	−0.5000	16(2)	1.00
		$CuGeO_3$-IV at 7.6 GPa			
Ge(1)	0.500(8)	0.2958(7)	0.731(3)	6(4)	1.00
Cu(1)	0.000	0.5000	0.000	9(9)	1.00
Cu(2)	0.000	0.0000	0.000	9(9)	1.00
O(1)	0.110(40)	0.369(4)	0.749(11)	20(30)	1.00
O(2)	0.690(40)	0.188(5)	0.012(8)	22(19)	1.00
O(3)	0.360(30)	0.044(5)	0.690(6)	18(30)	1.00

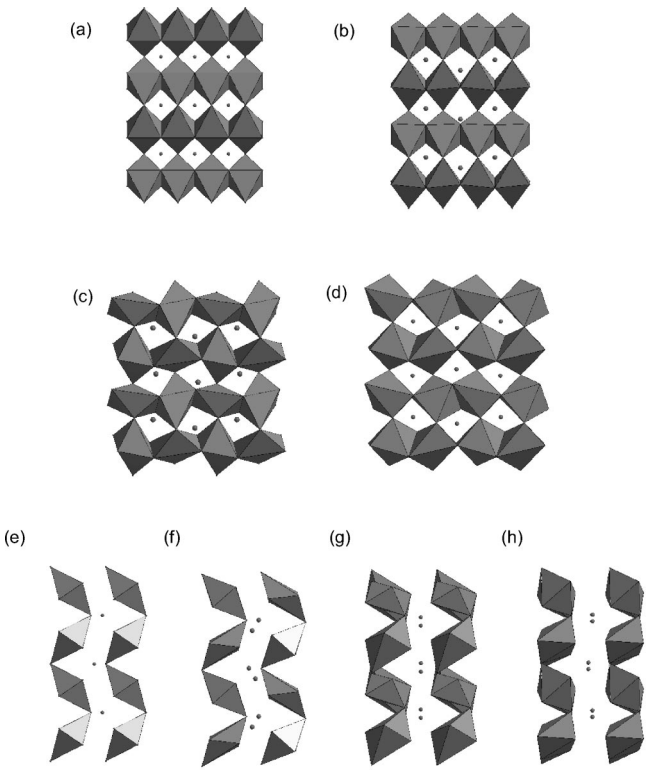

FIG. 2. The Cu-substructure in $CuGeO_3$ viewed along **a** [(a)–(d)] for phases I (a), III (b), IV (c), and II (d); (e)–(g) present views along **c**. The polyhedra represent Cu coordination, the small balls Ge^{4+} ions.

$CuGeO_3$-I individual chains of CuO_6 octahedra are separated from each other in the direction normal to the rippled layers by chains of GeO_4 tetrahedra The Ge chains are formed by sharing of all four tetrahedral vertices; two are shared with the vertices of adjacent tetrahedra to form pyroxenelike one-dimensional chains of the ''einer'' type,[16] and two are shared with the vertices of two different CuO_6 octahedra (the tetrahedral site will hereafter be referred to as the T^1 site). It is worth noting that in $CuGeO_3$-I there are two unoccupied tetrahedral sites (T^2 and T^3) that share faces with T^1 tetrahedra. These two unoccupied tetrahedra form one-dimensional chains with the same topology as the T^1 chains, and are also arranged in such a way that pairs of tetrahedra form distorted trigonal bipyramids as a result of the face-sharing orientation ($TB^1 = T^1 + T^2$ and $TB^2 = T^1 + T^3$).

The transformation of $CuGeO_3$ from phase I to phase III results in a doubling of the *a* and *c* unit-cell edges, while the *b* axis remains unchanged. The *a* in $CuGeO_3$-III is 4.7% elongated, compared to $CuGeO_3$-I, while *b* and *c* are shorter by 3.3% and 1.6%, respectively. The density of phase III is slightly higher (0.4%) than that of phase I. On the basis of Raman experiments, a ''zweier'' geometry of Ge chains has been suggested for phase III.[16] Indeed, in $CuGeO_3$-III we find corner-shared tetrahedral chains where Ge atoms occupy alternating T^1 and T^2 sites. Consequently, the translational symmetry between neighboring trigonal bipyramids is broken, as there are now two symmetry-independent trigonal bipyramids: one containing sites Ge(11) and Ge(12), and the other containing sites Ge(21) and Ge(22) both with the equatorial planes located at the *a* glide plane (010), as illustrated in Fig. 3(b). The apical oxygen atom in the trigonal bipyramids of phase I has now split into two symmetry-independent sites [O(2) and O(5)], each serving as the apical oxygen atom for the two symmetry-independent trigonal bipyramids of $CuGeO_3$-III. Tetrahedra along the pyroxenelike chains are oriented such that each tetrahedron sits with one edge along the line defining the chain direction, in a manner similar but not equivalent to the ''zweier-type'' pyroxene chain. If the equatorial planes of the pseudotrigonal bipyramids within a chain are taken as a reference, the structure of the chain may be described as an alternating pattern of GeO_4 tetrahedra, one above the plane, and the next below the plane, as shown in Fig. 3(b). Chains stacked one above the other form layers perpendicular to the [001] direction. The adjacent chains are not connected by any shared vertices. In this arrangement, sites Ge(22) and Ge(12) are located inside T^1 tetrahedra, while the Ge(11) and Ge(21) sites sit in the T^2 tetrahedral sites. Each GeO_4 tetrahedron is also in contact with four neighboring CuO_6 octahedra; T^1 shares all vertices with four octahedra, and T^2 shares two edges and four corners with three neighboring octahedra. Two additional atomic positions partially filled by Ge atoms correspond to inverse Ge layers.

Rippled layers of CuO_6 octahedra in $CuGeO_3$-III retain the same topology as in phase I, with all Cu atoms octahedrally coordinated, as shown in Fig. 2(b). The I-III transformation affects the Cu atoms in two ways. First, the rear-

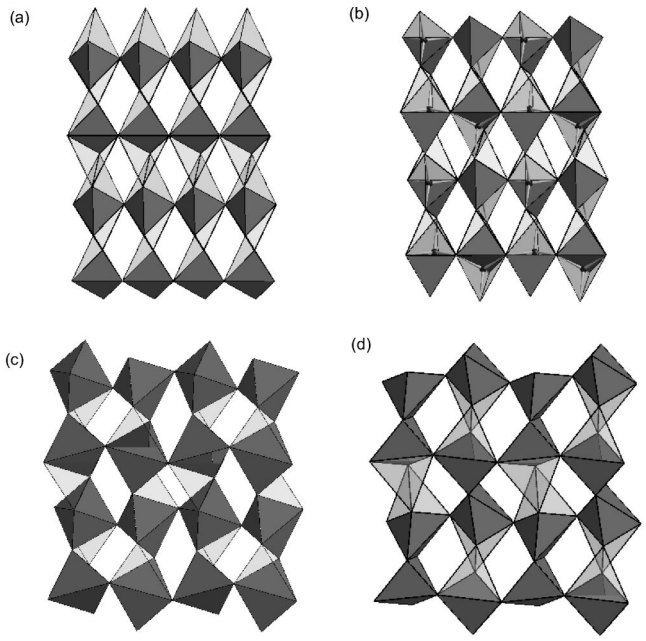

FIG. 3. The Ge substructure in $CuGeO_3$ viewed along **a** [(a)–(d)] for phases I (a), III (b), IV (c), and II (d). The solid polyhedra represent Ge coordination, the transparent polyhedra unoccupied tetrahedral sites. The balls and sticks inside transparent tetrahedra in (b) represent partially occupied Ge sites corresponding to inverse Ge layers.

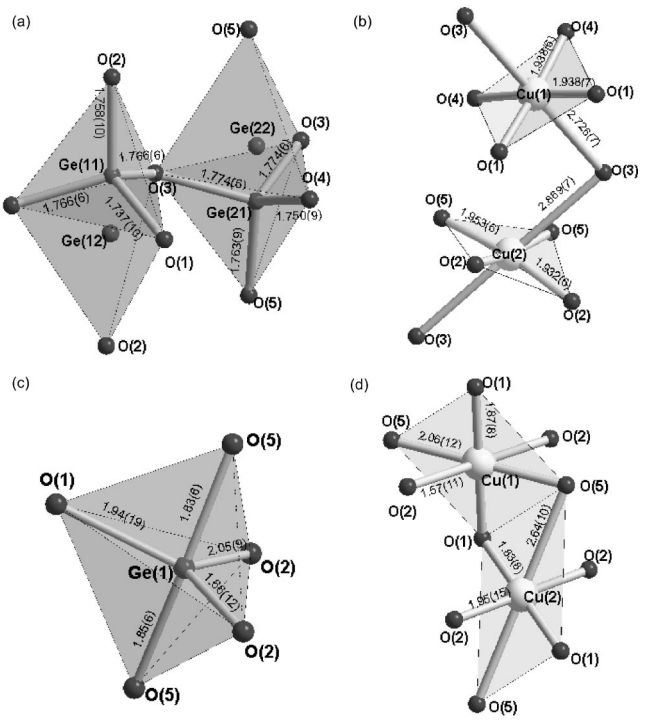

FIG. 4. The coordination geometry of $CuGeO_3$: (a) GeO_4 tetrahedra in $CuGeO_3$-III; (b) CuO_6 octahedra in $CuGeO_3$-III; (c) GeO_5 bipyramids in $CuGeO_3$-IV; (d) CuO_6 octahedra in $CuGeO_3$-IV.

rangement of layers of GeO_4 tetrahedra dictates the degree to which the octahedral layers can fold. Second, the alternation between occupation of T^1 and T^2 sites introduces a distinction between the two different types of chains that make up the whole layer. In $CuGeO_3$-III there are two symmetry-independent CuO_6 octahedra forming separate chains. Octahedra at Cu(2) share two edges and all corners with neighboring GeO_4 tetrahedra, whereas Cu(1) octahedra, similar to Cu(1) in phase I, share with only the corners with their adjacent GeO_4 tetrahedra. Apical oxygen atoms from the CuO_6 octahedra of phase I retain their role in $CuGeO_3$-III, whereas the equatorial oxygen atoms from phase I become split in phase III between O(1) and O(4) in the Cu(1) chain and O(2) and O(5) in the Cu(2) chain.

B. Geometry of coordination polyhedra in $CuGeO_3$-III

Distances between alternative tetrahedral sites for Ge atoms (corresponding to proper and inverse layers) in $CuGeO_3$-III are 1.06(2) Å for Ge(11) and Ge(12), and 1.00(2) Å for Ge(21) and Ge(22). These short distances make the simultaneous occupation of the two adjacent sites unlikely as a result of the large electrostatic repulsion that would certainly develop. Distances between neighboring Ge atoms on the same side of the equatorial plane of the trigonal bipyramidal site (of which only one may be occupied at any time, according to our model) are 2.898(1) Å for both Ge(11)-Ge(22) and Ge(12)-Ge(22) pairs. These values are smaller than the Ge-Ge distance of 3.081(1) Å in the folded configuration of the Ge chain in phase III, supporting the conclusion that the main structural change in the transition from phase I to phase III, i.e., the rearrangement of the chains of GeO_4 tetrahedra, is directed toward the elimination of strong Ge-Ge repulsion. The resulting chains consequently contain shorter Ge-O bonds, as can be seen in Fig. 4(a). Average values of bond angles for all GeO_4 tetrahedra are close to the ideal tetrahedral value. Divalent copper represents a classic case of the Jahn-Teller distortion. Typically, the shortening of the four equatorial bonds is matched by a lengthening of the two axial bonds that is twice the distance by which the equatorial bonds are shortened. In La_2CuO_4,[32] for example, the equatorial bonds measure 1.907 Å, while the axial distances are 2.465 Å. For comparison, the equatorial and axial distances in $CuGeO_3$-I are 1.942 and 2.756 Å, respectively. The coordination about the Cu atom in $CuGeO_3$-I therefore appears to represent an unusual case of the Jahn-Teller effect, due to the quite long axial Cu-O distances. Consequently, there has been some discussion in recent years concerning the nature of the distortion of the CuO_6 octahedron,[6,22] and whether or not the distortion of the CuO_6 octahedron is really an example of the Jahn-Teller effect, or whether the coordination environment at Cu is simply a result of the unusual arrangement of tetrahedral GeO_4 in the oxide structure. It is important to point out, however, that perfect D_{4h} symmetry is maintained about the CuO_6 octahedron in $CuGeO_3$-I, despite the strong electrostatic attraction of the tetravalent Ge atom for the equatorial oxygen atoms. In this regard, there is nothing unusual about the coordination of the Cu atom in $CuGeO_3$-I; it is possible, however, that lower-order structural effects, in addition to the Jahn-Teller distortion, may contribute to the unusually long axial Cu-O distances in the structure. In $CuGeO_3$-I the bend-

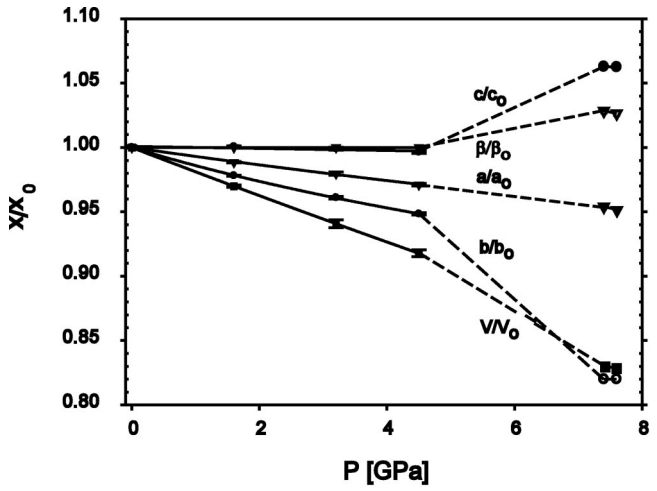

FIG. 5. Isothermal compressibility of $CuGeO_3$-III, with phase transition to $CuGeO_3$-IV at about 7 GPa. The black triangles after phase transition correspond to $a/2a_0$.

ing of the two-dimensional sheets of CuO_6 octahedra along the axial direction is quite severe at the apical oxygen atom [the Cu-O(1)-Cu angle is 100.5°]. This indicates that the bonding interaction between Cu dz^2 and O $2p$ orbitals along that direction will be reduced, since the bonding orbitals of the Cu dz^2-O$2p$ band located at the oxygen atom will not have their optimum 180° overlap. It is therefore expected that the bond length will increase along with the bending of the CuO_6 sheets in that direction. After the transition from phase I to phase III, the same topology of CuO_6 octahedra is preserved, but the average Cu-O axial length increases to 2.797(7) Å, while the angle at the apical oxygen atom decreases to 94.1(2)° accordingly, as illustrated in Fig. 4(b). In phase III, the octahedra are also somewhat distorted from D_{4h} symmetry as a result of the changing occupation patterns of the GeO_4 tetrahedra, which in turn affect the equatorial Cu-O bonds. The O-Cu-O angles of the octahedra remain unaffected, however, and retain their ideal value of 180°. In both phase I and phase III, it is thus clear that the Jahn-Teller effect plays a dominant role in determining the coordination environment of the CuO_6 octahedron.

C. Isothermal compressibility

The elastic properties of $CuGeO_3$-III have been studied by monitoring changes in unit-cell parameters (four different pressures for phase III and two pressures for phase IV). The results of fitting the Murnaghan equation of state,[33] which was used to calculate the elastic moduli of phase III, to the experimental data, are presented in Fig. 5. In our experiments the precision of pressure determination was about 0.1 GPa. The availability of only four pressure points in the phase-III region is sufficient to estimate the compressibility, but is rather too limited to reliably determine curvature. Therefore, in our fits of the equation of state, the K', which describes the curvature, was fixed to 4.

There is a significant discrepancy between the values of elastic moduli for $CuGeO_3$ phase I presented by different authors.[4,21,22,24] The comparison of elastic properties of $CuGeO_3$-I and $CuGeO_3$-III is presented in Table III. The bulk modulus for $CuGeO_3$-III is $K_0=52.47(3)$ GPa, and $CuGeO_3$-III is more rigid than $CuGeO_3$-I. We found that the maximum compressibility direction in phase III is the crystallographic **b** direction, within the Cu plane, perpendicular to the chain direction. The compressibility is significantly lower than in phase I, as a result of the change in the configuration of Ge chains. As in phase I the least compressible direction is along the **c** axis. The only direction that is more compressible in phase III is **a**, the direction perpendicular to the layers. The III-IV phase transition has almost no effect on the pressure dependence of *a*, whereas the other lattice parameters are affected strongly. As a result of the transformation *c* expands by about 4%, and *b* contracts by about 10%. There is also a 3% drop in the volume of the equivalent unit cell.

TABLE III. Comparison of elastic moduli for $CuGeO_3$-I and $CuGeO_3$-III. Data for $CuGeO_3$-I are from Brauniger *et al.* (Ref. 22).

Data	K_0 (GPa)	
	$CuGeO_3$-I	$CuGeO_3$-III
V	39.5(30)	52.47(3)
a	201(40)	141(12)
b	49.2(45)	66(1)
c	845(240)	1242(600)

D. Crystal structure of $CuGeO_3$-IV

Hydrostatic compression of $CuGeO_3$-III results in the formation of $CuGeO_3$-IV, whose structure is closely related to that of $CuGeO_3$-II, the nonquenchable phase formed upon hydrostatic compression of $CuGeO_3$-I.[4] Upon decompression, both phase II and phase IV transform to their respective precursor phases and not, as might be expected, to a single energetically favorable phase.

In phase IV, the topology of the rippled layers of CuO_6 octahedra is preserved, as shown in Fig. 2(c). Because there is no room in this compressed structure for the empty spaces (i.e., the unoccupied tetrahedral sites of $CuGeO_3$-III) the main structural feature driving the III-IV transformation is a change in Ge coordination from tetrahedral to pseudotrigonal bipyramidal. In this process, the Ge atoms assume an approximately symmetrical position that lies in between the two face-sharing tetrahedral sites of $CuGeO_3$-III, causing the inverse layers present in the structure of phase III to become identical with proper layers. The trigonal bipyramidal coordination of Ge^{4+}, similar to that reported for $CuGeO_3$-II,[4] although not very common, is not unusual. It has been found, e.g., in some open-framework germanates.[34–36] Correspondingly, a formation of a five-coordinated silica phase upon nonhydrostatic compression has also been proposed by theoretical predictions.[37,38] In $CuGeO_3$-IV pressure has the added effect of condensing the tetrahedral framework. In $CuGeO_3$-III, the one-dimensional chains of GeO_4 tetrahedra are not connected, but in $CuGeO_3$-IV, these chains now share a corner, and there is only one symmetry-independent

TABLE IV. Topology of Ge layers in different high-pressure polymorphs of $CuGeO_3$.

Phase	Ge^{+4} coordination number	Ge-layer topology
I	4	$-T^1-T^1-T^1-T^1-$
		$-T^1-T^1-T^1-T^1-$
		$-T^1-T^1-T^1-T^1-$
III	4	$-T^1-T^2-T^1-T^2-$
		$-T^1-T^2-T^1-T^2-$
		$-T^1-T^2-T^1-T^2-$
IV	5	$-TB^1-TB^2-TB^1-TB^2-$
		$-TB^1-TB^2-TB^1-TB^2-$
		$-TB^1-TB^2-TB^1-TB^2-$
II	5	$-TB^1-TB^2-TB^1-TB^2-$
		$-TB^2-TB^1-TB^2-TB^1-$
		$-TB^1-TB^2-TB^1-TB^2-$

type of trigonal bipyramidal site, as is the case in phase I. The topology of Ge chain can be described as "$-TB^1$-TB^2-" chains, with the same $-TB^1$-TB^2- sequence of the adjacent chains within a layer. The topology of Ge layers in phase II, on the other hand, is based on the same type of $-TB^1$-TB^2- chain, but adjacent chains have the inverse sequence $-TB^2$-TB^1-, as illustrated in Fig. 2 and summarized in Table IV. The repulsion energy that develops between Cu atoms on compression, as well as the change in coordination of Ge in $CuGeO_3$-IV, make it energetically unfavorable for phase IV to maintain a parallel configuration of the octahedral chains. As a result, the chains of CuO_6 octahedra assume an even more folded form than in phase III, as pairs of equatorial oxygen atoms are pushed away from the Cu atoms on either side of the shared edge. Whereas in $CuGeO_3$-III, the two symmetry-independent Cu atoms form separate chains (neighboring chains within the same layer are symmetry independent), $CuGeO_3$-IV contains two symmetry-independent sites, but the chains are no longer composed of symmetry-equivalent octahedra, and neighboring polyhedra within the same chain are now symmetry independent. As a result, there is only one symmetry-independent pair of equatorial ligands to be shared between neighboring edge-sharing octahedra.

E. Geometry of coordination polyhedra in $CuGeO_3$-IV

As described in the preceding sections, Ge atoms in phase IV are five-coordinated, corresponding to a distorted trigonal bipyramid. Each Ge polyhedron shares two edges with one of the octahedra in a neighboring chain of CuO_6. Within each trigonal bipyramid, equatorial bonds measure 2.05(9), 1.94(19), and 1.66(12) Å, while the apical distances are 1.83(6) and 1.85(6) Å, as shown in Fig. 4(d).

As in $CuGeO_3$-III, there are two symmetry-independent Cu sites in $CuGeO_3$-IV, and the octahedral coordination about each is maintained through the III-IV phase transition. The distinction between the two sites is, however, more pronounced in phase IV than in phase III, as illustrated in Fig. 4(d). While the coordination about Cu(1) strongly resembles the CuO_6 octahedra of phase III, Cu(2) has a rather unusual distortion. It appears to be that the very dramatic distortion present in phase III is being suppressed. The two axial bonds are becoming noticeably shorter, and two of the equatorial bonds are becoming longer with compression. Although the typical Jahn-Teller effect observed in divalent copper gives rise to "four short + two long" bond distortion of the ideal octahedron, the alternative choice, the "two short + four long" arrangement is degenerate to first order with the former. It is only second-order considerations that make the former choice almost universally observed in copper oxides.[39] Therefore it is possible to drive the Jahn-Teller distortion back to the alternative "four long + two short" pattern, if uniaxial stress is allowed by the atomic environment around this Cu atom. As in phase III, the Jahn-Teller distortion of the CuO_6 octahedron is modified by the coordination requirements of the Ge polyhedra; in this particular case, the compression pathways of the two symmetry-inequivalent CuO_6 octahedra are also clearly different, and the application of hydrostatic pressure to the whole crystal produces different behavior at the atomic level. While the Jahn-Teller distortion of the Cu(1) site is merely enhanced by pressure, the distortion of the Cu(2) site appears to be dramatically altered. Yoshiasa *et al.*[4] reported an unusually short O-O distance of 2.14 Å in phase II. The shortest O-O distance in $CuGeO_3$-IV [2.434 Å for O(3)-O(2)] is much more reasonable. Another striking feature of $CuGeO_3$-II is the fact that Ge bipyramids in adjacent chains share edges, which results in a very short Ge-Ge distance of 2.917 Å, the shortest among all the phases [2.943 Å in $CuGeO_3$-I, 3.081 Å in $CuGeO_3$-III, and 3.139(26) Å in $CuGeO_3$-IV]. It is not clear to us why a structure with such a strong electrostatic repulsion would be favored during hydrostatic compression over more relaxed structures of nonhydrostatic phases. Taking into account the topological similarity between phases II and IV, the structure model for $CuGeO_3$-II seems justified, but the unusual geometry of this phase requires further confirmation by more precise studies.

F. Effect of nonhydrostaticity and metastability of high-pressure phases

The topology of Cu layers in $CuGeO_3$ is preserved throughout all the pressure-induced phase transformations discussed in this paper. Therefore understanding the properties of Cu layers is essential for explaining the high-pressure behavior of $CuGeO_3$. Cu^{2+} is a strongly Jahn-Teller distortion susceptible ion and can participate in cooperative Jahn-Teller effect-induced phase transitions.[40] Also, the coordination sphere of Cu^{2+} in octahedral complexes is known to deform easily and this seems to be the underlying cause of their plasticity.[41] Copper metagermanate is an extremely soft material and undoubtedly this property derives from the deformability of CuO_6 octahedra in the structure. The fact that the Ge ions can move from one tetrahedral site to another (in phases II, III, and IV) and rotate with relative ease,[6] suggests that there should be more stable configurations at ambient pressure. It seems noteworthy that recent molecular-dynamics calculations on silica[37,38] indicate that in the pres-

ence of deviatoric stress new polymorphs can be obtained. In particular, these studies have shown that a silica polymorph with fivefold coordinated Si may be produced under certain conditions. Although the existence of penta-SiO_2 has not been confirmed experimentally, these results show that deviatoric stress may cause configurations that are not accessible under isotropic compression, but become accessible under nonhydrostatic conditions. We think that with very soft and highly plastic crystalline materials, such as $CuGeO_3$, differences in behavior under hydrostatic and nonhydrostatic conditions may be a rule rather than an exception. In our experiments we were not able to quantitatively specify the deviatoric stress. We are, however, certain that a strong uniaxial stress was acting along the [100] crystallographic direction, perpendicular to the layers in $CuGeO_3$. Although understanding of the effect of the uniaxial-stress direction on the phase transitions in $CuGeO_3$ would require further detailed studies, it seems possible that deviatoric stress and Jahn-Teller distortion may be working synergetically to stabilize metastable phases.

All the pressure-induced transformations that $CuGeO_3$ undergoes at pressures lower than 10 GPa can be explained with the use of a simple model. The basis of the model is adiabatic effective potential energy E_{el} of the crystal as a function of configuration of the Ge chain. The Ge^{4+} ions can assume positions inside any of the T^1, T^2, and T^3 tetrahedra, as well as between two tetrahedra, in trigonal bipyramidal coordination inside TB^1 or TB^2. There are several possibilities (polymorphic structures corresponding to local minima of E_{el}) for Ge ions to form chains with different symmetry and periodicity, but there seems to be a general rule. Namely, below about 7 GPa the structures with Ge^{4+} in fourfold coordination are more stable, whereas at higher pressure the trigonal bipyramidal coordination is favored. If we accept the models of phases III and IV, it becomes apparent that phase IV is actually an intermediate step of the I-III transformation, because the Ge^{4+} ions have to pass through the bipyramidal site occupied in phase IV in order to shift from T^1 to T^2 tetrahedra. By analogy one may expect a hypothetical phase IIa to exist, related to phase II. In phase IIa every other Ge^{4+} ion would be shifted to the terahedral site in another half of the bipyramid occupied in phase II. For clarity we will not consider all the E_{el} minima, and will concentrate on the main five of them, corresponding to phases I, II, IIa, III, and IV. At low pressure E_{el} has the form of an asymmetrical five-well function. The global minimum corresponds to $CuGeO_3$-I. The E_{II} and E_{IIa} minima are separated from E_{III} and E_{IV}, which means that the direct transitions such as II-III, IIa-III, II-IV, and IIa-IV are not plausible. As pressure increases the E_{el} changes shape, as schematically shown in Fig. 6. On compression (independent of the hydrostaticity) the relation between E_I and the rest of the minima changes, with E_I gradually becoming shallower. At pressure close to 6.5 GPa, E_I is no longer the deepest minimum. Between 6.5 and 7.0 GPa, E_{el} minima corresponding to phases IIa and III become deepest, and E_I shallowest. However, the energy barriers E_{I-IV} and E_{I-II} are still higher than the thermal energy E_T. At higher pressure the height of these barriers decreases and a phase transformation to either E_{II} or E_{IV} is thermally activated. The hydrostaticity seems to have an effect mainly on the height of the energy barriers, but also determines which of these two paths is assumed. If the transition point is reached during nonhydrostatic compression, the barrier E_{IV-III} is lower than the thermal energy E_T and the structure transforms through phase II to phase III. It is necessary that the thermal activation of the I-IV transition (and immediately further the IV-III transition) becomes possible at pressure when the energy levels are already reversed ($E_{III}<E_I$), and not the opposite, because in the latter case $CuGeO_3$-III would not be quenchable. In the case of hydrostatic compression the path through E_{II} is energetically favorable, but the E_{II-IIa} barrier is too high and the transformation proceeds to a metastable phase II instead of IIa. On further slight pressure increase phases II and IV, with five-coordinated Ge, become deepest minima, and in the case of nonhydrostatic compression III-IV transformation occurs. On pressure release, $CuGeO_3$-IV transforms first to $CuGeO_3$-III, then E_{I-IV} becomes higher than E_T, and finally, E_I regains the global minimum role, but due to insufficient E_T the E_{I-III} barrier cannot be crossed and $CuGeO_3$-III is metastably quenched. When phase III is subjected to increased temperature the E_{el} does not change significantly. At a level where E_T becomes higher than E_{I-III} crossing of the barrier becomes possible and the crystal assumes the configuration corresponding to lowest energy minimum of $CuGeO_3$-I. During hydrostatic decompression of phase II, E_{IIa} is still not accessible because of the high-energy barrier and transformation proceeds to phase I.

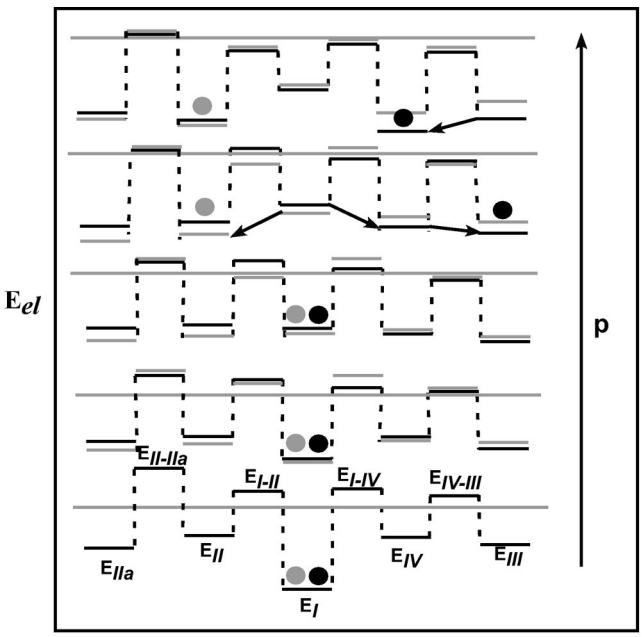

FIG. 6. The changes in effective adiabatic potential energy as a function of Ge-chain configuration during hydrostatic (gray line) and nonhydrostatic (black line) compression. The circles describe the structure stable (metastable) at given pressure during compression at ambient temperature. The horizontal arrows indicate phase transitions.

The metastability model presented above has important, experimentaly verifiable consequences for the pressure-temperature behavior of $CuGeO_3$.

(i) If the temperature during nonhydrostatic compression is low enough the formation of phase III should be supressed. There is already an experimental evidence for this phenomenon. In the high-pressure–low-temperature studies[14,15] formation of phases III and IV was not observed at low temperature up to a pressure of 8.2 GPa, despite the use of different pressure media (He, Ar, alcohol mixture) all of which were solid at the temperatures of the experiments.

(ii) If the hypothesis about the E_{el} deepest minimum change prior to thermal activation of I-III phase transition is correct, it should be possible to induce this transition at nonhydrostatic pressure lower than 7 GPa by just heating the sample (provided that heating will not anneal the sample and restore hydrostaticity). This effect has yet to be confirmed experimentally.

IV. CONCLUSIONS

It is evident from studying the evolution of $CuGeO_3$ from phase I to phase III and from phase III to phase IV that the two-dimensional layers of CuO_6 octahedra remain intact, and that the primary structural change accompanying the transitions among $CuGeO_3$ polymorphs is the change in the occupation of the tetrahedral sites. $CuGeO_3$-III is quenchable to ambient conditions, and it is natural to conclude that, compared to the structure of phase I, the more open framework of phase III is energetically favorable. When a crystal of pressure-quenched $CuGeO_3$-III is heated to 600°, however, the kinetic energy is apparently high enough to allow the Ge atom to pass between the triangular face of the face-shared pair of tetrahedral sites and on to the other tetrahedral void. At elevated temperatures in $CuGeO_3$-I, the chains of GeO_4 tetrahedra contain noticeably longer Ge-Ge distances, which in turn reduces the electrostatic repulsion, making phase I the global thermodynamic minimum, despite the fact that phase III is quenchable to ambient conditions. In phase III, the T^1 and T^2 chains are occupied alternately, and since the transition from phase III to phase IV with pressure requires a change in the Ge coordination number from 4 to 5, the Ge atom at T^2 can only assume a position inside TB^1 (the trigonal bipyramid formed between tetrahedral sites T^1 and T^2), as T^2 shares a face only with T^1. On the other hand, Ge atoms at T^1 sites can move to either TB^1 or TB^2 (the trigonal bipyramid formed between tetrahedral sites T^1 and T^3). The energetic preference in this case should be with TB^2 since this would allow an increased Ge-Ge distance along the chain of GeO_4 tetrahedra to be greater than if only TB^1 bipyramids were occupied. As a result, the structure of phase IV contains only one type of trigonal bipyramid.

The crystal structures of $CuGeO_3$-III and $CuGeO_3$-IV presented above throw interesting light on the understanding of the complicated phase behavior of copper metagermanate. Based on this information, it should be possible to quantitatively interpret the available high-pressure Raman spectra for phases II, III, and IV. We also hope that the models proposed here will stimulate theoretical studies that may provide answers to the questions about the energetics of different phases and the effect of nonhydrostatic conditions.

ACKNOWLEDGMENTS

We wish to thank S. W. Cheong of Lucent Technologies for preparing the single crystals of $CuGeO_3$, R. J. Hemley for stimulating discussions on this problem, and C. L. Cahill for a revision of the manuscript. This study was primarily supported by funding from NSF grant EAR9973018. Support from Center for High Pressure Research (CHiPR) is also acknowledged.

[1] M. Hase, I. Terasaki, and K. Uchinokura, Phys. Rev. Lett. **70**, 3651 (1993).
[2] H. Voellenke, A. Wittmann, and H. Nowotny, Monatsch. Chem. **98**, 1352 (1967).
[3] M. Braden, E. Ressouche, B. Buchner, R. Kessler, G. Heger, G. Dhalenne, and A. Revcolevschi, Phys. Rev. B **57**, 11 497 (1998).
[4] A. Yoshiasa, G. Yagyu, T. Ito, T. Yamanaka, and T. Nagi, Z. Anorg. Allg. Chem. **626**, 36 (2000).
[5] I. Yamada, M. Nishi, J. Akimitsu, J. Phys.: Condens. Matter **8**, 2625 (1996).
[6] M. Hidaka, M. Hatae, I. Yamada, M. Nishi, and J. Akimitsu, J. Phys.: Condens. Matter **9**, 809 (1997).
[7] O. Kamimura, M. Terauchi, M. Tanaka, O. Fujita, and J. Akimitsu, J. Phys. Soc. Jpn. **63**, 2467 (1994).
[8] K. Hirota, D.E. Cox, J.E. Lorenzo, G. Shirane, J.M. Tranquada, M. Hase, K. Uchinokura, H. Kojima, Y. Shibuya, and I. Tanaka, Phys. Rev. Lett. **73**, 736 (1994).
[9] J.P. Pouget, L.P. Regnault, M. Ain, B. Hennion, J.P. Renard, P. Veillet, G. Dhalenne, and A. Revcolevschi, Phys. Rev. Lett. **72**, 4037 (1994).
[10] M. Nishi, O. Fujita, J. Akimitsu, K. Kakurai, and Y. Fujii, Phys. Rev. B **52**, R6959 (1995).
[11] S. Katano, O. Fujita, J. Akimitsu, and M. Nishi, Phys. Rev. B **52**, 15 364 (1995).
[12] H. Takahashi, N. Mori, O. Fujita, J. Akimitsu, M. Matsumoto, Solid State Commun. **95**, 817 (1995).
[13] G. Quirion, F.S. Razavi, B. Dumoulin, M. Poirier, A. Revcolevschi, and G. Dhalenne, Phys. Rev. B **58**, 882 (1998).
[14] A.R. Goni, T. Zhou, U. Schwarz, R.K. Kremer, and K. Syassen, Phys. Rev. Lett. **77**, 1079 (1996).
[15] P.H.M. van Loosdrecht, J. Zeman, G. Martinez, G. Dhalenne, and A. Revcolevschi, Phys. Rev. Lett. **78**, 487 (1997).
[16] A. Jayaraman, S.K. Sharma, S.Y. Wang, and S.-W. Cheong, Curr. Sci. **71**, 306 (1996).
[17] A. Jayaraman, S.K. Sharma, S.Y. Wang, and S.-W. Cheong, Phys. Rev. B **55**, 5694 (1997).
[18] A. Jayaraman, S.Y. Wang, L.C. Ming, and S.-W. Cheong, Phys. Rev. Lett. **75**, 2356 (1995).
[19] There has been confusion concerning the naming of the ambient-

temperature high-pressure phase III obtained by quasihydrostatic compression (Ref. 18), and the low-temperature high-pressure phase III (Ref. 15). These phases have very different Raman spectra. Throughout this paper we refer to the former as $CuGeO_3$-III, and the latter as $CuGeO_3$-I′. It should also be noted that some authors (Refs. 14 and 15) used for the nonhydrostatic phases III and IV the the names IIa and IIb. In this case we are following the convention introduced by Jayaraman *et al.* (Ref. 18).

[20] A preliminary single-crystal XRD study on quenched phase III by Kulkarni *et al.* (unpublished) indicated an orthorhombic cell with similar lattice parameters, and yielded atomic positions consistent with the shifting of the alternate GeO_4 tetrahedra in the chains. However, the resulting *R* factor was too high (>10%) to accept the structure model obtained. Indeed, this prompted the present study.

[21] D.M. Adams, J. Haines, and S. Lenard, J. Phys.: Condens. Matter **3**, 5183 (1991).

[22] S. Brauninger, U. Schwarz, M. Hanfland, T. Zhou, R.K. Kremer, and K. Syassen, Phys. Rev. B **56**, R11 357 (1997).

[23] M. Braden, B. Buchner, S. Klotz, W.G. Marshall, M. Behruzi, and G. Heger, Phys. Rev. B **60**, 9616 (1999).

[24] L.C. Ming, S.R. Shieh, A. Jayaraman, S.K. Sharma, and Y.H. Kim, J. Phys. Chem. Solids **60**, 69 (1999).

[25] G.M. Sheldrick, SHELXTL, University of Goettingen, Germany, 1997.

[26] Y. Mizuno, T. Tohyama, and S. Maekawa, Phys. Rev. B **60**, 6230 (1999).

[27] M. Matsuda, K.M. Kojima, Y.J. Uemura, J.L. Zarestky, K. Nakajima, K. Kakurai, T. Yokoo, S.M. Shapiro, and G. Shirane, Phys. Rev. B **57**, 11 467 (1998).

[28] A. Shengelaya, G.I. Meijer, J. Karpinski, G.-M. Zhao, H. Schwer, E.M. Kopnin, C. Rossel, and H. Keller, Phys. Rev. Lett. **80**, 3626 (1998).

[29] M. Baenitz, C. Geibel, M. Dischner, G. Sparn, F. Steglich, H.H. Otto, M. Meibohm, and A.A. Gippius, Phys. Rev. B **62**, 12 201 (2000).

[30] R. Neudert, H. Rosner, S.-L. Drechsler, M. Kielwein, M. Sing, Z. Hu, M. Knupfer, M.S. Golden, J. Fink, N. Nucker, M. Merz, S. Schuppler, N. Motoyama, H. Eisaki, S. Uchida, M. Domke, and G. Kaindl, Phys. Rev. B **60**, 13 413 (1999).

[31] H. Rosner, S.-L. Drechsler, K. Koepernik, R. Hayn, and H. Eschrig, Phys. Rev. B **63**, 073104 (2001).

[32] B. Grande, Hk. Mueller-Buschbaum, and M. Schweitzer, Z. Anorg. Allg. Chem. **428**, 120 (1977).

[33] R.J. Angel, in *Comparative Crystal Chemistry*, edited by R.M. Hazen and R.T. Downs (MSA, Washington, D.C., 2001).

[34] A. Tripathi, V.G. Young, G.M. Johnson, C.L. Cahill, and J.B. Parise, Acta Crystallogr., Sect. C: Cryst. Struct. Commun. **55**, 496 (1999).

[35] M.S. Dadachov, K. Sun, T. Conradsson, and X. Zou, Angew. Chem. Int. Ed. Engl. **39**, 3674 (2000).

[36] K. Sun, M.S. Dadachov, T. Conradsson, and X. Zou, Acta Crystallogr., Sect. C: Cryst. Struct. Commun. **56**, 1092 (2000).

[37] J. Badro, J.-L. Barrat, and P. Gillet, Phys. Rev. Lett. **76**, 772 (1996).

[38] J. Badro, D.M. Teter, R.T. Downs, P. Gillet, R.J. Hemley, and J.-L. Barrat, Phys. Rev. B **56**, 5797 (1997).

[39] J.K. Burdett and J.F. Mitchell, J. Am. Chem. Soc. **112**, 6571 (1992).

[40] I.B. Bersuker, *The Jahn Teller Effect and Vibronic Interactions in Modern Chemistry* (Plenum Press, New York, 1984).

[41] J. Gazo, Coord. Chem. Rev. **19**, 253 (1976).